TECHNICAL PAPER

# Friction Stir Lap Welding Ti–6Al–4V Alloy Using a Threaded Pin by Simulation and Experimental Investigation

**Zhenlei Liu**[1] · **Kang Yang**[1] · **Yumei Yue**[1] · **Dejun Yan**[2]

**Abstract** Commonly, the rotating tool during friction stir welding of Ti–6Al–4V alloy owns flat surfaces since serious tool wear always appears during welding. However, a tool with flat surface easily results into insufficient material mixing during friction stir lap welding process. In order to increase material mixing between the upper and lower sheets while welding Ti–6Al–4V alloy, a tool with a threaded pin was used in this work. The material flow behaviors at the lap interfaces using pins with and without threads were investigated. Results showed that when using the threaded pin, the maximum material flow velocity showed an obvious increase at the lap interface, which was beneficial to enhance the material mixing between upper and lower sheets. Even using the threaded pin, void-like defects appeared at joint bottoms using higher rotating speeds of 200 and 180 rpm, which were eliminated by decreasing the rotating speed to 150 rpm because of reduced temperature gradient along sheet thickness direction. The welding processes in this work were considered as below β-transus temperature because no obvious lamellar structures were observed on all the joints. The maximum failure load of 20.23 KN was attained when using 200 rpm. The lap joints presented tensile fracture mode.

## 1 Introduction

Ti–6Al–4V alloy is one of the most common two phase (α + β) titanium alloys. Ti–6Al–4V alloy owns various advantages due to high strength, good corrosion resistance and high temperature strength. Ti–6Al–4V alloy has been widely used in aviation, aerospace and ship building industries [1]. Similar to aluminum and its alloys, Ti–6Al–4V alloy joints fabricated by fusion welding always have defects of coarse microstructures, hot cracks, high residual stresses [2]. Friction stir welding (FSW) is invented by The Welding Institute (TWI) in the 1990s. As a solid state joining method, lots of fusion defects can be avoided during FSW. FSW has been gaining a plenty of attentions since invention [3–7]. Therefore, FSW seems suitable to join Ti–6Al–4V alloy.

Up till now, some investigations about the microstructure and mechanical properties of Ti–6Al–4V alloy FSW joints have been done and some important conclusions have been yielded [7–10]. Zhou et al. [7] found that when the stir zone (SZ) of FSW joint was characterized by fully lamellar microstructure, joint tensile properties decreased with increasing tool rotating speed. Su et al. [8] found that lower rotational speed and higher welding speed resulted into higher joint tensile strength. Using rotating speeds from 50 to 150 rpm, Yoon et al. [9] obtained FSW joints below β-transus temperature. Edwards et al. [10] welded Ti–6Al–4V alloy sheets of different thicknesses and obtained extremely small heat affected zone (HAZ). Furthermore, microstructure and mechanical properties of

Zhenlei Liu and Kang Yang have contributed equally to this work.

✉ Yumei Yue
  sau_yueyumei@163.com

1 Faculty of Aerospace Engineering, Shenyang Aerospace University, Shenyang 110136, People's Republic of China

2 Guangdong Key Laboratory of Enterprise Advanced Welding Technology for Ships, CSSC Huangpu Wenchong Shipbuilding Company Limited, Guangzhou 510715, People's Republic of China

back heating assisted Ti–6Al–4V alloy FSW were investigated by Ji et al. [11, 12].

Friction stir lap welding (FSLW) joint is another typical joint type of FSW. FSLW joints are used in airplane panels, wing frames and floor decks [13]. FSLW joint is formed by first plunging a tool into two or more overlapped sheets and then moving forward the tool along a predetermined line. So far, numerous studies about FSLW of aluminum and magnesium alloys have been reported [14–16]. Naik et al. [14] lap welded AZ31B–H24 Mg alloy and reported that hooking defects significantly reduced the fatigue strength because of the stress concentration and reduced effective sheet thickness (EST) of the upper sheet. Yang et al. [15] used different tools to join AZ31 magnesium plates and found that a triangular-morphology pin effectively suppressed hook and resulted in 78% increase of joint strength. But, studies about FSLW of Ti–6Al–4V alloy are relatively few [17, 18].

The rotating tool used during welding is the main factor affecting the material flow behavior. The thread on pin is the main factor affecting the material mixing between upper and lower sheets. However, because of the low thermo-plasticity of Ti–6Al–4V alloy, tool bears big torque and wear during FSW [19]. Hence, the tools without thread have always been used in the Refs. [3, 7, 8]. Few papers about tool optimization during FSW or FSLW of Ti–6Al–4V alloy have been reported. In this study, to increase the material mixing of the upper and lower sheets during FSLW, a tool with a threaded pin was used. Using different rotating speeds, the microstructure and mechanical properties of the lap joints were mainly discussed.

## 2 Experiment

Ti–6Al–4V alloys were used as the base materials (BMs) of this work. The thicknesses of upper and lower sheets were respectively 1 and 1.8 mm. The sheets were cut into 300 mm × 140 mm. All sheets were cleaned with emery papers to wipe off oxidation layers before welding. During welding, the FSW-3LM-4012 machine was used. Different rotating speeds of 200, 180 and 150 rpm and a constant welding speed of 30 mm/min were chosen. The welding parameters were chosen based on our previous experience to obtain satisfied joint formation [11, 12, 18]. A W-25% Re rotating tool with a threaded pin was used, as shown in Fig. 1. The tool had a concave shoulder and the shoulder diameter was 12 mm. The diameter of the pin tip and root were respectively 3 and 5.5 mm. The length of the pin was 1.8 mm. The thread width and depth were 0.5 and 0.3 mm, respectively. The thread pitch was 1.5 mm. Argon gas shielding was continuously sprayed on the joint surface



Fig. 1 Rotating tool with a threaded pin used in the present study

during welding. Shoulder plunge depth was chosen as 0.2 mm and the tilting angle was 2.5°.

After welding, the metallographic samples and lap shear specimens were cut using an electrical discharge cutting machine. The width of lap shear specimens was 20 mm. Metallographic specimens were then polished and etched. Microstructure analysis was performed on an optical microscope (OM, Olympus–GX71) and a scanning electron microscope (SEM, SU3500) after etching using Kroll reagent (13 ml HF + 26 ml $HNO_3$ + 100 ml $H_2O$). Lap shear tests were performed using a constant speed of 5 mm/min. The fracture positions were observed using a stereoscopic microscope (ZSA403). The fracture surfaces were observed using the SEM.

## 3 Model Description

### 3.1 Solid Model and Mesh Generation

To testify the advantage of the threaded pin, a traditional smooth tool was used in simulation. The material flow behaviors using the two pins were simulated. The dimensions of the threaded pin tool in simulation were the same as the dimensions of the smooth pin. The traditional tool owned the same morphology and corresponding dimensions besides the threading. The tool models used in simulation are shown in Fig. 2. The tool models were built using CATIA software. The finite element generation was fulfilled by Gambit software [20]. In gambit, the mesh element was Tet/Hybrid type and the mesh spacing was chosen as 0.1 mm. During simulation, the dimensions of the plate were 300 mm × 140 mm × 2.8 mm, representing lap joint whose upper and lower thicknesses were 1 and 1.8 mm, respectively.

**Fig. 2** Tool models: **a** the traditional flat tool and **b** the tool with a threaded pin
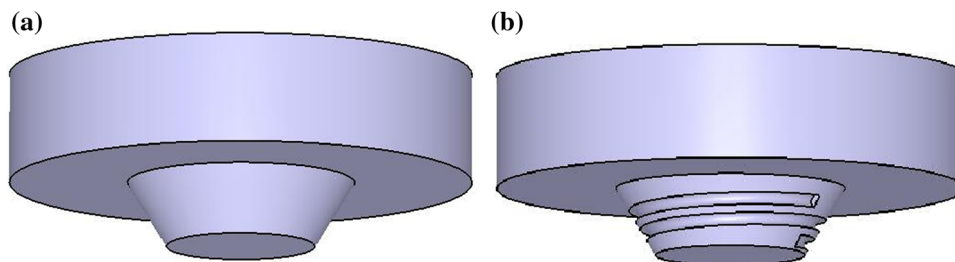
### 3.2 Material Parameters and Boundary Conditions

In simulation, the mass of Ti–6Al–4V alloy was 4450 kg/m$^3$. The values of specific heat, thermal conductivity and viscosity were the same with the Ref. [21], which were 879 J/(kg K), 15.91 W/(m K) and 5.3 mPa s. During welding, the material at the SZ was considered as fluid. The right side of the plate was assumed to be the fluid inlet. The fluid inlet had a velocity value of 30 mm/min. The front and back, upper and lower plates were assumed to be walls, which owned the same velocity as the welding speed. The left side of the plate was assumed to be the fluid outlet. Shoulder and pin surfaces were supposed to be rotational walls, whose velocities were consistent with the rotating velocity of the pin. In simulation, the rotating speed of 200 rpm was chosen. The rotating direction was the same as the tool. The simulation model is shown in Fig. 3.

## 4 Results and Discussion

### 4.1 Simulation Results

The three-dimensional material flow field and the material flow behavior at the lap interface have been analyzed. The distance from joint upper surface to the lap interface was
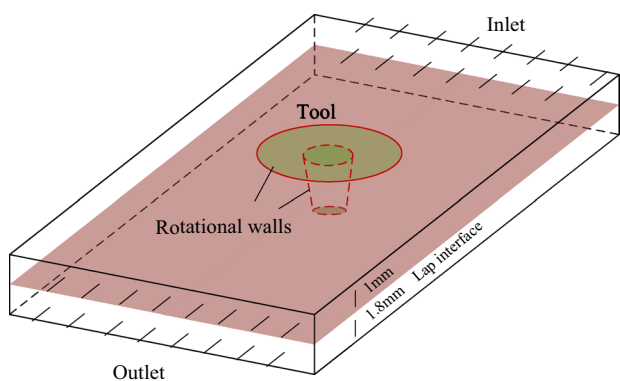


**Fig. 3** Simulation model of this work

1 mm, which was equal to the thickness of the upper sheet. The schematic of the lap interface is shown in Fig. 3.

The material flow behaviors using the two pins are shown in Fig. 4. Figure 4a, b show the three-dimensional material flow behaviors. The maximum flow velocity was attained near the shoulder edge region, which was characterized by the red lines. The maximum velocities using the two different tools were similar. This was because the shoulder diameters of the two tools were the same. Figure 4c, d show the material flow behaviors of the lap interfaces at 200 rpm. The maximum flow velocity using the threaded pin was 0.049 m/s, which was higher than 0.044 m/s using the smooth pin. It was observed that the material adjacent to the threads in Fig. 4d also owned bigger flow velocity. The material flow behaviors of the two pins using 180 and 150 rpm are shown in Fig. 4e–h. It was observed that the maximum velocities using the threaded pin were bigger than those using the smooth pin. This result proved that the threaded pin was beneficial to increase the flow velocity of the lap interface.

### 4.2 Joint Cross Section Morphologies

The joint cross sections using different rotating speeds are shown in Fig. 5. The joint cross section presented a typical basin-like morphology. Small flashes and shoulder marks were observed at the joint surfaces. With increasing the rotating speed from 200 to 150 rpm, the joint morphology showed little change. At the AS of the joint, the original lap interface showed an upward bending morphology, which was called hook. At the retreating side (RS) of the joint, the lap interface was characterized by dark lines across the SZ, which was called cold lap.

Figure 6a shows the hook using the threaded pin. The hook height was about 175 μm, showing that adequate material mixing happened. Figure 6b shows the cold lap using the threaded pin tool. It was observed that the cold lap showed a downward morphology due to the big forging force of the tool shoulder. Some small voids were observed inside the cold lap. When using relatively high rotating speed of 200 and 180 rpm, small voids were observed at joint bottoms (Fig. 6b, c). This defect was eliminated by using a rotating speed of 150 rpm, (Fig. 6d). Some researchers such as Su

**Fig. 4** Material flow behavior: three-dimensional flow fields using the smooth **a** and threaded pins **b**, material flows at the interfaces **c** smooth and **d** threaded pins at 200 rpm, **e** smooth and **f** threaded pins at 180 rpm, **g** smooth and **h** threaded pins at 150 rpm
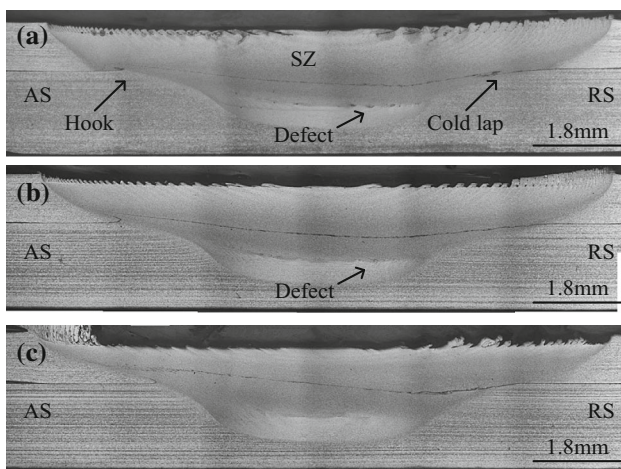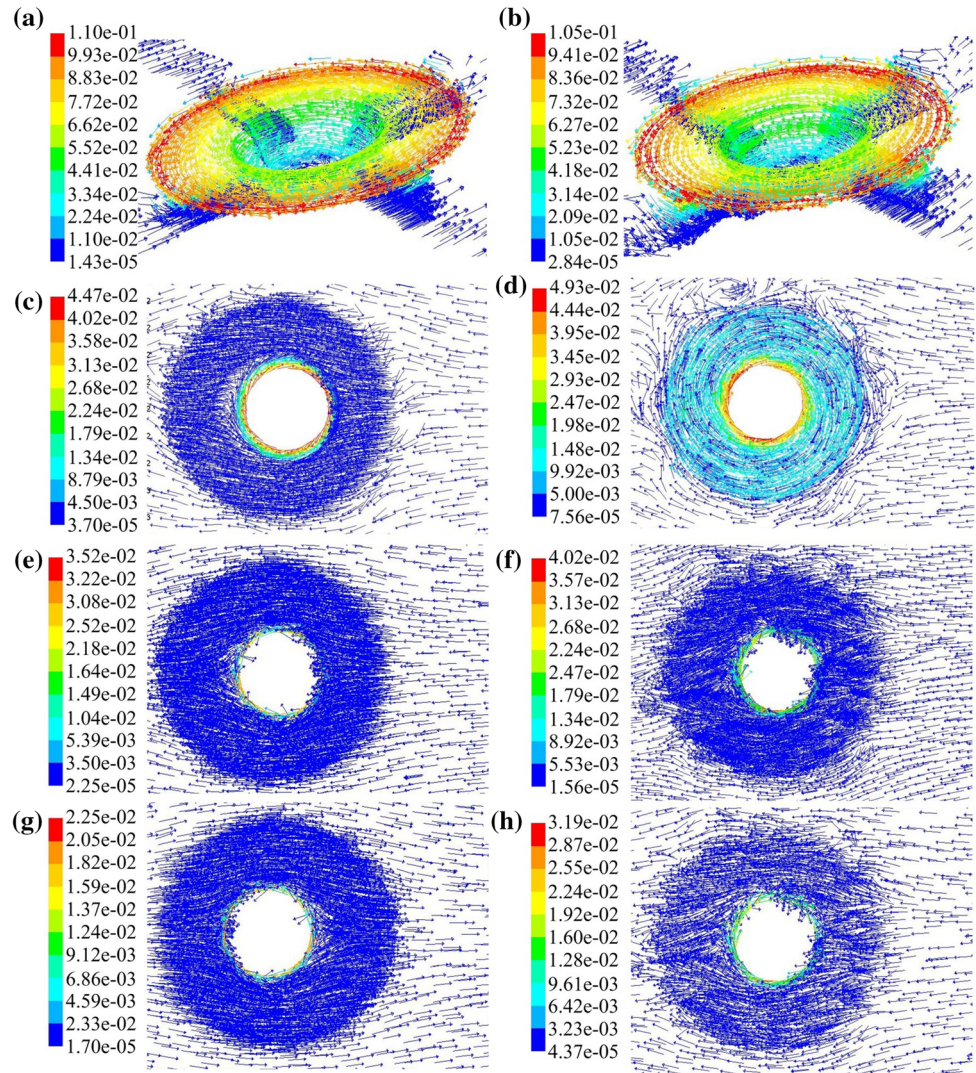
**Fig. 5** Joint cross sections using: **a** 200 rpm, **b** 180 rpm and **c** 150 rpm

et al. [8] and Mironov et al. [22] attributed the voids to insufficient material softening, while Ji et al. [11, 12] attributed the voids to big temperature gradient along the sheet thickness direction. Void defects at joint bottoms of aluminum alloy FSW joints were due to insufficient material flow behavior. The void of this paper was obtained at higher rotating speed, showing that the main reason was not material flow behavior. The authors believed that the welding peak temperature and big temperature gradient along thickness were the main reason [11, 12].

### 4.3 Microstructure of Lap Joints

Figure 7 shows the BM microstructure of Ti–6Al–4V alloy, which was characterized by primary α and transformed β phases. The α and β phases showed gray and white morphologies under SEM. As discussed previously and similar to butt joint, big temperature gradient was formed along thickness while welding Ti–6Al–4V alloy.

**Fig. 6** Hooks and cold laps:
**a** hook and **b** cold lap and defect
at 200 rpm, **c** cold lap and
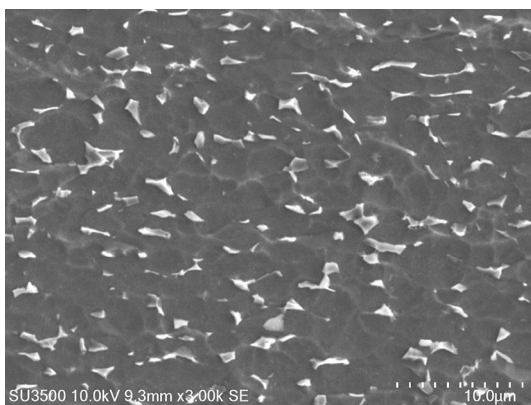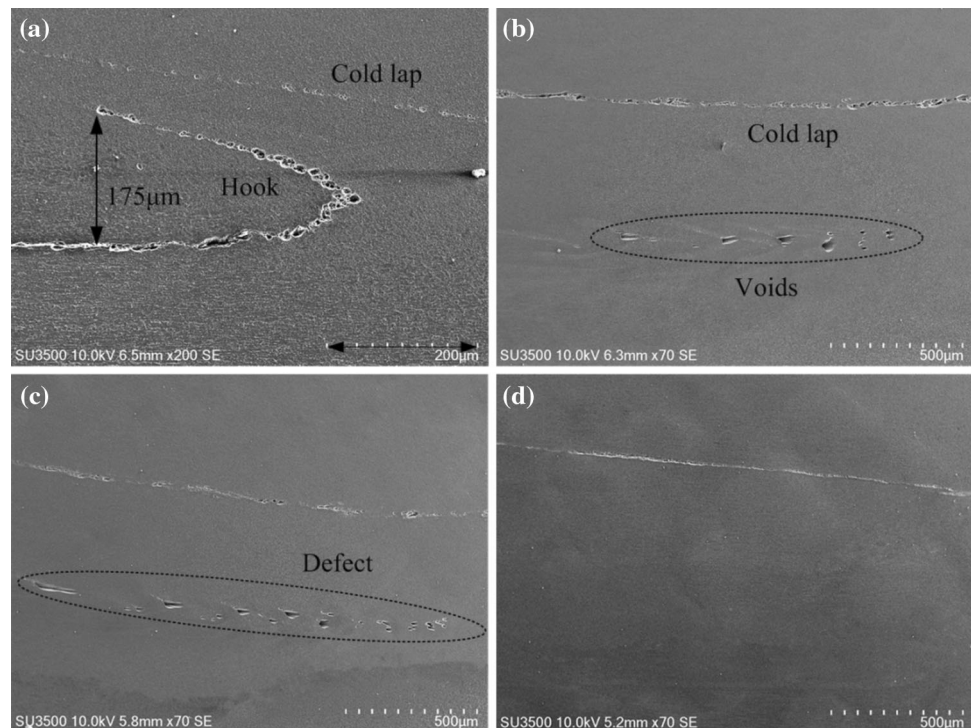defect at 180 rpm, **d** cold lap at
150 rpm



**Fig. 7** Microstructure of the BM

Hence, different microstructures were obtained in this work since Ti–6Al–4V alloy is a two phases ($\alpha + \beta$) titanium alloy. To fully understand this, the microstructures along thickness using different rotating speeds were compared, as shown in Fig. 8. The microstructures of the SZ top regions are shown in Fig. 8a–c. Some small lamellar $\alpha/\beta$ was observed in Fig. 8a, showing that the $\beta \rightarrow \alpha + \beta$ transformation occurred and this process happened during the cooling stage. Besides, the microstructure in Fig. 8a shows that the peak temperature was still below $\beta$-transus temperature. Using 180 and 150 rpm, the main phases were $\alpha$. The equiaxed grains in Fig. 8b, c reveal that dynamic recrystallization happened during welding. Figures 8d–f respectively show the microstructure at the SZ bottom regions. Only fine and equiaxed grains were observed.

## 4.4 Lap Shear Failure Load of the Lap Joints

Figure 9 shows the lap shear failure loads of the joints. It was seen that with decreasing the rotating speed, the average lap shear failure load gradually decreased. The maximum failure load of 20.23 KN was attained when at 200 rpm. The minimum failure load of 18.77 KN was attained at 180 rpm. The fracture position of the joint is shown in Fig. 10. Only one fracture mode was observed: tensile fracture mode. Crack first initiated from the hook tip, then propagated through the SZ and finally reached the joint upper surface. For FSLW joints, effective sheet thickness (EST) was always used to qualify effect of hook or cold lap on joint lap shear properties. As shown in Fig. 6, the hooks in this work showed upward bending morphologies. Hence, when the joint was subjected to external loads, crack more easily propagated along the hook. The tensile fracture mode meant excellent material mixing between the upper and lower sheets. However, the hook heights were similar (Fig. 5), meaning that the ESTs using different rotating speeds were similar. Therefore, the lap shear properties of joints were mainly determined by the microstructures. The peak temperatures using the three rotating speeds were below $\beta$-transus temperature (In Fig. 8). Thus the joint mechanical properties were mainly determined by the $\alpha$ phases. The crack first propagated through the upper sheet, namely the SZ middle regions during tests. Figure 11 shows the grains at the middle region of the joints. The sizes of the $\alpha$ phases using
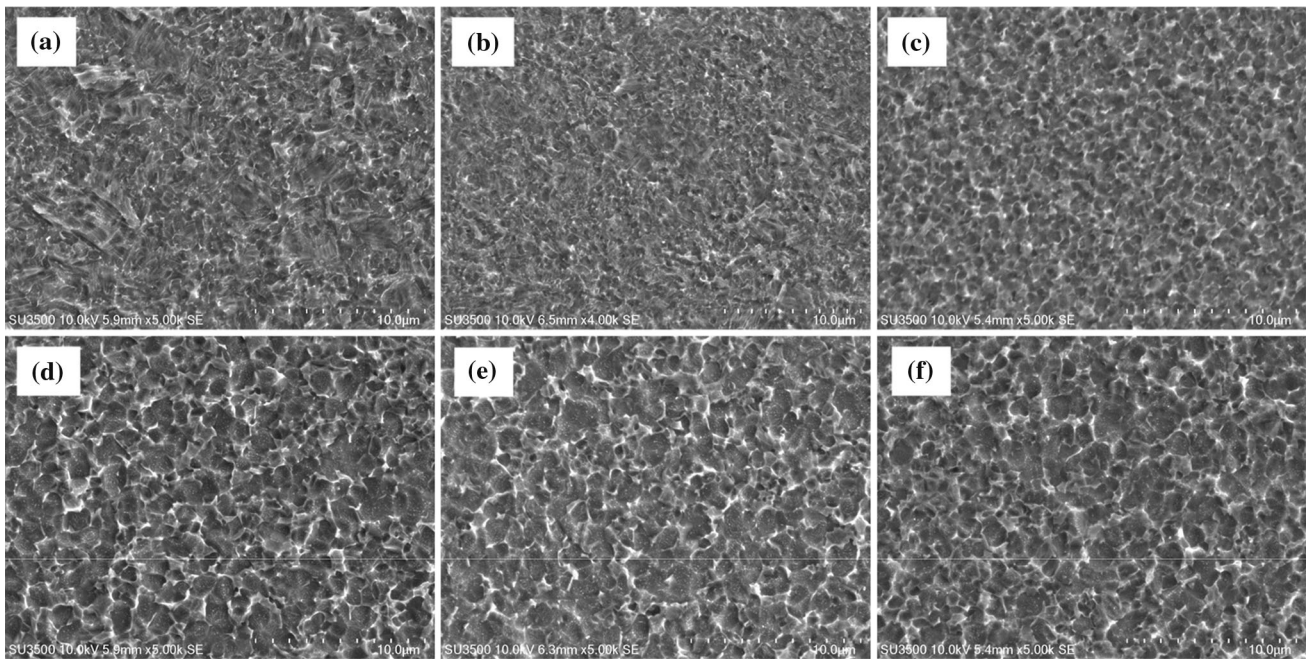
Fig. 8 Microstructure along thickness **a–c** SZ top regions at 200, 180 and 150 rpm, **d–f** SZ bottom regions at 200, 180 and 150 rpm
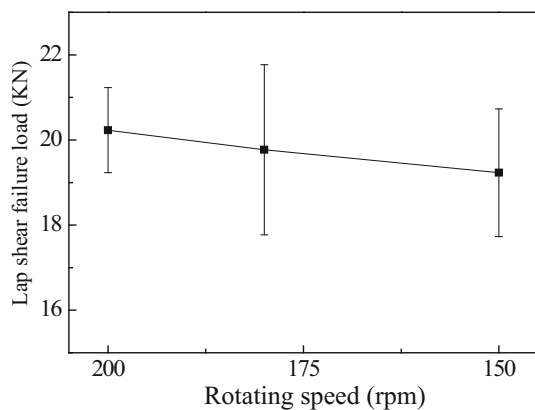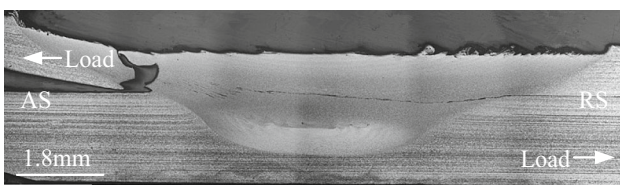


Fig. 9 Lap shear failure loads of the joints



Fig. 10 Fracture position

200 rpm were slightly smaller than those using 180 and 150 rpm. Possible reason for this was more violent mechanical stirring induced by higher rotating speed. As is well known, smaller grain sizes were beneficial for the increase of the mechanical properties [9]. Hence the joint using 200 rpm owned bigger failure loads.

### 4.5 Fracture Morphologies

Figure 12 shows the fracture morphology. The testing position was the SZ of the joint. Numerous dimples were observed in Fig. 12a. Figure 12b shows the magnified view of the fracture surface. It was observed that the dimples were rather small and shallow. The sizes of the dimples were small because of the small grain sizes at the SZ. Generally, the fracture surface indicated ductile fracture mode.

## 5 Conclusions

This study focused on increasing the material mixing between the upper and lower sheets during FSLW of titanium alloy Ti–6Al–4V. Using a threaded pin, the microstructure and lap shear failure load of the lap joints were investigated. The simulation method was used to compare the material flow behaviors using the threaded and traditional smooth pins. The following conclusions were drawn.

1. The simulation results showed that the threaded pin increased the material flow at the lap interface.
2. A void-like defect, which was formed because of the big temperature gradient along thickness, was observed at joint bottom when using 200 rpm. By decreasing the rotating speed, temperature gradient decreased, and therefore, the size of defect became smaller.

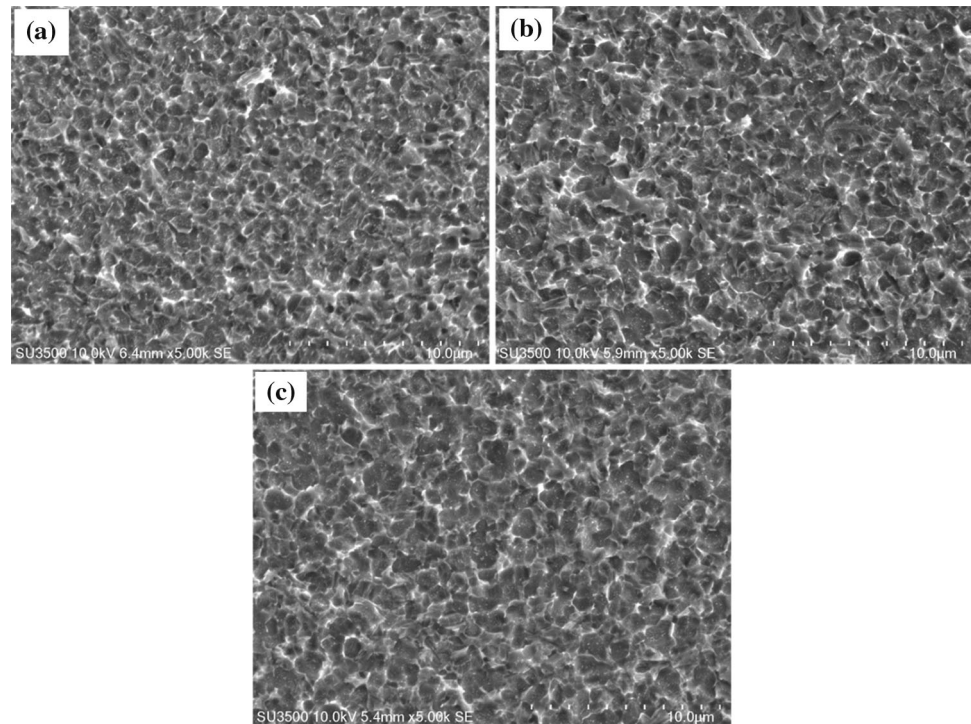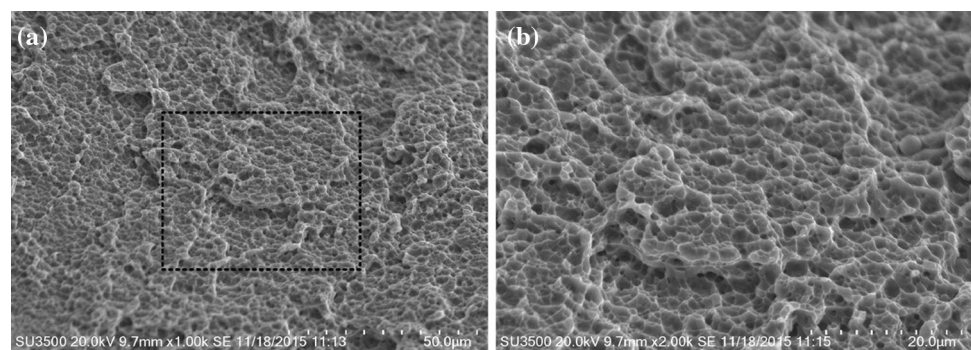**Fig. 11** Grains of the SZ middle using: **a** 200 rpm, **b** 180 rpm and **c** 150 rpm



**Fig. 12** Fracture morphologies of joint **a** and its magnified view **b**



3. Microstructure showed difference along thickness due to big temperature gradient. When using 200–150 rpm, welding peak temperatures were below β-transus temperature.

4. With decreasing the rotating speed from 200 to 150 rpm, lap shear failure load gradually decreased. The maximum failure load of 20.23 KN was obtained using 200 rpm.

## References

1. Davies P S, Wynne B P, Rainforth W M, Thomas M J, and Threadgill P L, *Metall Mater Trans A* **42** (2011) 2278.

2. Zhang Z H, Li W Y, Feng Y, Li J L, and Chao Y J, *Acta Mater* **92** (2015) 117.

3. Kitamura K, Fujii H, Iwata Y, Sun Y S, and Morisada Y, *Mater Des* **46** (2013) 348.

4. Salari E, Jahazi M, Khodabandeh A, and Ghasemi-Nanes H, *Mater Des* **58** (2014) 381.

5. Cantin G M D, David S A, Thomas W M, and Lara-Curzio E, *Sci Technol Weld Join* **10** (2005) 268.

6. Cui L, Yang X, Xie Y, Hou X, and Song Y, *Mater Des* **51** (2013) 161.

7. Zhou L, Liu H J, and Liu Q W, *Mater Des* **31** (2010) 2631.

8. Su, J Wang J, Mishra R S, Xu R, and Baumann J A, *Mater Sci Eng A* **573** (2013) 67.

9. Yoon S, Ueji R, and Fujii H, *J Mater Process Technol* **229** (2016) 390.

10. Edwards P D, and Ramulu M, *Sci Technol Weld Join* **14** (2009) 476.

11. Ji S, Li Z, Wang Y, and Ma L, *Mater Des* **113** (2017) 37.

12. Ji S, Li Z, Zhang L, and Wang Y, *Mater Lett* **188** (2017) 21.

13. Song Y B, Yang X Q, Cui L, Hou X P, Shen Z K, and Xu Y, *Mater Des* **55** (2014) 9.

14. Naik B S, Chen D L Cao X, and Wanjara P, *Metall Mater Trans A* **44A** (2013) 3732.
15. Yang Q, Li X, Chen K, and Shi Y J, *Mater Sci Eng A* **528** (2011) 2463.
16. Cao X, and Jahazi M, *Mater Des* **32** (2011) 1.
17. Buffa G, Fratini L, Schneider M, and Merklein M, *J Mater Process Technol* 213 (2013) **2312**.
18. Xu Z, Li Z, Lv Z, and Zhang L, *Int J Adv Manuf Technol* (2016) https://doi.org/10.1007/s00170-016-9741-7.
19. Wang J, Su J, Mishra R S, Xu R, and Baumann J A, *Wear* **321** (2014) 25.
20. Li Z, Yue Y, Ji S, Peng C, and Wang L, *Mater Des* **94** (2016) 368.
21. Ji S, Zou A, Yue Y, Luan G, and Jin Y, *Acta Metallurgica Sinica (English Letters)* **299** (2012) 365.
22. Mironov S, Sato Y S, and Kokawa H, *Acta Mater* **57** (2009) 4519.